How is Charge Transport Different in Ionic Liquids? : Effect of High Pressure

Published in:
Phys. Chem. Chem. Phys.

Document Version:
Peer reviewed version

Queen's University Belfast - Research Portal:
Link to publication record in Queen's University Belfast Research Portal

PCCP

ARTICLE

How is Charge Transport Different in Ionic Liquids? : Effect of High Pressure

Z. Wojnarowska,* [a,b] E. Thoms, [a,b] B. Blanchard, [a,b] S. N. Tripathy, [a,b] P. Goodrich,[c] J. Jacquemin,[c] J. Knapik[ab] and M. Paluch* [a,b]

Modern ionic liquids (ILs) are magical green solvents for the future due to their inherited advantages and remarkable transport properties. One of the ubiquitous properties in ILs is the intrinsic ionic conductivity. However, the understanding of super-Arrhenius behavior of ionic conductivity process at elevated pressure still remains elusive and crux in glass science. In this work, we investigate the ion transport properties of 1-butyl-3-methylimidazolium bis[(trifluoromethyl)sulfonyl]imide: [C₄mim] [NTf₂], 1-butylimidazolium bis[(trifluoromethyl)-sulfonyl]imide: [C₄Him] [NTf₂] and 1-butylimidazolium hydrogen sulfate: [C₄Him] [HSO₄] ILs in supercooled liquid state using dielectric spectroscopy at ambient and high pressure. We present the experimental data in the dynamic window of conductivity formalism to examine the charge transport properties. The frequency-dependent ionic conductivity data have been analyzed using the time-temperature superposition principle. In the Arrhenius diagram, thermal evolution dc-conductivity reveals similar temperature dependence for both protic and aprotic ILs thus making it difficult to distinguish the ion dynamics. However, our results demonstrate the key role of high pressure that unambiguously separates the charge transport properties of protic ILs from aprotic ones through apparent activation volume paramterer. We also highlight that the activation volume can be employed to assess the information connecting the ability of ionic systems to form H-bond networks and the impact of proton transfer involved in the conduction process.

Key Words: Ionic liquid, dc-conductivity, high pressure, activation volume.

I. Introduction

Arguably, the understanding of ion relaxation and diffusion in interacting or cooperatively relaxing systems remains the major physical quest in material chemistry.[1-5] These systems include all kinds of glass forming supercooled liquids, including ionic conductors. [5-10] In this context, fluids that are largely made of ions and short-lived ion pairs, such as ionic liquids (ILs) enjoy elevated technological interest. By definition, ILs exhibit a melting temperature (T_m) below ~ 100 °C to distinguish them from inorganic molten ionic conductors.[1,3,11,12] Besides, ILs show extraordinary properties compared to the liquids whose molecular components are predominantly neutral such as water and toluene. The cations in ILs generally consist of a bulky organic structure of low symmetry, whereas the anions are inorganic or organic compounds that have a negative charge. As liquid salts, ILs are dominated by strong electrostatic interactions between ions and show unique physical properties, such as low melting points, low vapor pressure, non-flammability, thermal and chemical stability and broad electrochemical window.[8,11,13] This makes them potentially ideal as solvents and electrolytes.[3,14,15] The vast majority of ILs incorporate cations of unitary charge that are created from a neutral substrate by the net addition of a proton (H^+) or an alkyl chain (R^+) to the heteroatom lone pair. Those ILs formed by proton transfer (H^+) between an equimolar mixture of a Brønsted acid and a Brønsted base in the absence of any solvent are called 'protic' ILs (PILs), whereas their R^+ counterparts are considered to be 'aprotic' ILs (AILs). [11,13,16,17,18] Thus, the major difference between PILs and AILs is the presence of an exchangeable proton. Intriguingly, this can produce hydrogen bonding between an acid and base and in some cases creates an H-bonded extended network. The literature reports two types of charge transport mechanisms in protic ionic conductors: (a) vehicle and (b) Grotthuss-type. In the former one, the proton transfer is coupled or concomitant with the molecular diffusion (or viscosity); while in the latter, it is realized through the proton migration in the hydrogen bonded networks. These features result in an exceptionally high intrinsic ionic conductivity of protic ionic systems under anhydrous conditions and thus makes them elite candidates for industrial applications such as energy storage and electrochemical devices. Thus, a wide variety of ILs have already been designed by suitable combination of various cations with numerous anions to attain a wide spectrum of optimum properties.[19-24]

[a.] *Institute of Physics, University of Silesia, Uniwersytecka 4, 40-007 Katowice, Poland.*

[b.] *Silesian Center for Education and Interdisciplinary Research, 75 Pulku Piechoty 1A, 41-500 Chorzow, Poland.*
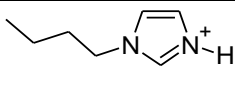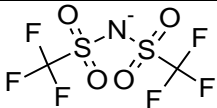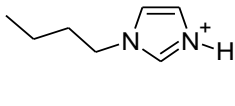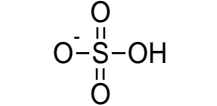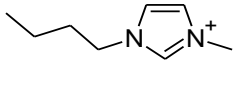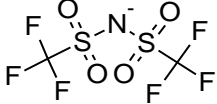
[c.] *The QUILL Research Centre, School of Chemistry and Chemical Engineering, Queen's University of Belfast, Stranmillis Road, Belfast BT9 5AG, United Kingdom.*

* Corresponding authors: zwojnaro@us.edu.pl , marian.paluch@us.edu.pl

ARTICLE

At this juncture, in order to appropriately employ these ILs in the most efficient manner, it is crucial to understand the transport or physical properties that determine the feasibility for a potential application. One of these ubiquitous properties in ILs is the inherent ionic conductivity which depends on a multitude of properties, *e.g.*, ion type, size, charge distribution, temperature and pressure. [24-31] As a consequence, many efforts have been devoted to understand the behavior of ionic conductivity relaxation and its mechanism in ILs at various thermodynamic conditions. It is well known that when an IL is cooled it often forms an ionic solid that may be crystalline or glassy.[7] As a consequence, the mobility of charge carriers slows down, resulting in a colossal drop of ionic conductivity (*i.e.*, up to 10 orders of magnitudes) between T_m and T_g. However, the transport properties near to T_g are not fully characterized and it is of interest to examine the dynamics of supercooled ILs obtained by both isobaric cooling and isothermal compression. The thermodynamic variable of pressure acts directly on the molecular packing and thus perturbs intermolecular interaction. As a result, the difference in transport properties between PILs and AILs can be suitably resolved. The focus of attention in this work is to study the conduction behavior of the following ionic liquids: (a) protic IL-[C4Him] [NTf2], (b) protic IL-[C4Him] [HSO4] and (c) aprotic IL-[C4mim] [NTf2][32] at ambient and elevated pressure (up to 600 MPa) using dielectric spectroscopy. This technique probes molecular fluctuations and measures the dielectric/electrical response over many orders of magnitude in frequency and in a wide temperature and pressure interval, proving to be the ideal experimental tool for this quest.[31] We will discuss the charge transport properties and conductivity scaling in these systems using a free energy random barrier model.[8,33] Special attention will be focused to understand the connection between activation volume parameter and the formation of the H-bonded network.

II. Experimental Details

Fig. 1 Chemical structures of the examined ILs

Ionic Liquid	Cation	Anion
[C4Him][NTf2]		
[C4Him][HSO4]		
[C4mim][NTf2]		

Materials

The sample tested herein are 1-butyl-3-methylimidazolium bis[(trifluoromethyl)sulfonyl]imide [C4mim] [NTf2], 1-butylimidazolium bis[(trifluoromethyl)sulfonyl]imide [C4Him] [NTf2] and 1-butylimidazolium hydrogen sulfate [C4Him] [HSO4].

These samples were synthesized and purified in-house in the QUILL Centre within a purity, expressed in mole fraction unit, greater than 0.99 as reported in the Electronic Supporting information (ESI). Prior to use, ILs were treated for 15 hours at 323.15 K under vacuum (lower than 1 Pa), the samples were then considered as dried and were then stored under a nitrogen atmosphere to avoid water contamination from the atmosphere. After this treatment, their halide content was determined using suppressed ion chromatography (IC), and the lithium content of the sample was then determined by inductively coupled plasma analysis (ICP). These measurements revealed very low levels of halide and lithium in each IL sample containing the [NTf2]- anion, which are less than to 20×10^{-6} and 25×10^{-6} in mass fraction units, respectively. The water content of the selected ILs determined by Karl Fischer titration varied with the protic ILs containing significantly higher levels of water than the aprotic IL. The molecular structure of ILs is shown in Figure 1 while the purity, molecular weight and impurities in each IL are tabulated in Table S1 of the ESI along with their ^{1}H and ^{13}C NMR spectra shown in Figures S1-S6 of the ESI.

Broadband dielectric spectroscopy (BDS)

Ambient pressure dielectric measurements of [C4Him] [NTf2], [C4Him] [HSO4] and [C4mim] [NTf2] were performed over a wide frequency range from (10^{-1} to 10^6) Hz using a Novo-Control GMBH Alpha dielectric spectrometer. During the measurements, the samples were placed between two stainless steel electrodes of the capacitor. The dielectric spectra were collected over the temperature range from (150 to 353) K and the data were presented in conductivity formalism. The temperature was controlled by the Novo-Control Quattro system, using a nitrogen gas cryostat. The temperature stability of the samples was better than 0.1 K.

For the pressure dependent BDS experiment the capacitor with each studied material was placed in the high-pressure chamber and compressed using the silicone fluid. The IL sample was in contact only with stainless steel and Teflon. The pressure was measured using a Nova Swiss tensometric pressure meter with a resolution of 0.1 MPa. The temperature was controlled within 0.1 K by means of a Weiss fridge.

Differential scanning calorimetry (DSC)

The standard differential scanning calorimetry measurements (DSC) of the selected ILs were performed using the Mettler-Toledo DSC apparatus equipped with a liquid nitrogen cooling accessory and a HSS8 ceramic sensor (heat flux sensor with 120 thermocouples). The temperature and enthalpy calibrations were carried out by indium and zinc standards. Prior the acquisition, each sample was supercooled at cooling rate 10 K min^{-1} to produce the amorphous material. In all the experiments, the DSC cell was purged with nitrogen at 60 mL min^{-1}. The thermal analysis was carried out between 370 K down to 150 K. The examined samples can be classified as good glass-forming liquids without any tendency toward crystallization.
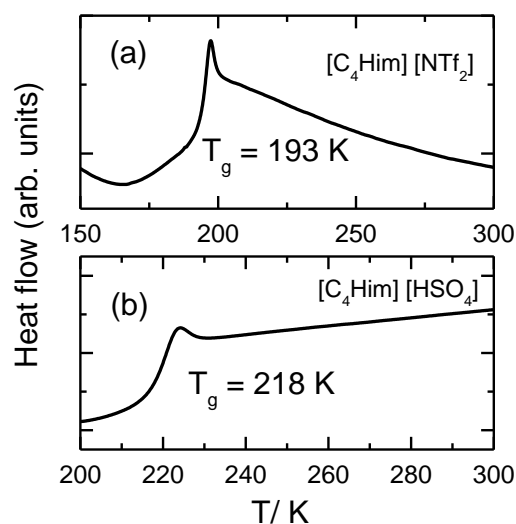
Journal Name

ARTICLE

Fig. 2 The DSC traces (endo up) for both protic ionic liquids **(a)** [C₄Him] [NTf₂] and **(b)** [C₄Him] [HSO₄].

Computational methods for calculating 3D structure of ILs and related properties

The sigma profile, COSMO volume and area of each species have been determined by using the COSMOthermX (version C30_1601) program package. Prior to determination of these 3D structural properties, the structure of each ion involved was optimized, with a convergence criterion of 10^{-8} Hartree in the gas phase, by using DFT calculations combining the Resolution of Identity (RI) approximation within the Turbomole 7.0 program package utilizing the B3LYP functional with the def-TZVP basis set. Each resultant optimized structure was then used as an input for the generation of the conformers of each species using the COSMOconfX program (version 4.0). Additionally, an estimation of the IL free volume is then calculated by taking the difference between the calculated molar volume and the COSMO volume of the IL using COSMOthermX.[34]

III. Results and Discussion

A. Glass transition temperature

To provide the preliminary characterization of glass transition dynamics, we present DSC measurements for ILs supercooled at the cooling rate of 10 K min⁻¹ in Figure 2. The DSC traces for both protic ionic liquids [C₄Him] [NTf₂] and [C₄Him] [HSO₄] exhibit well-defined glass transitions, characterized by the endothermic heat flow changes at T = 193 K and 218 K, respectively. Interestingly, the glass transition temperature data of the aprotic IL [C₄mim] [NTf₂], reported in the literature (T_g = 181.5 K) is lower than T_g for both PILs.[35] Furthermore, we note that the change of anion type from [HSO₄]⁻ to [NTf₂]⁻ has a greater impact on the glass transition temperature compared to a variation of cation, i.e., [C₄Him]⁺ → [C₄mim]⁺.

B. Charge transport at ambient pressure (p = 0.1 MPa)

The general molecular picture of charge transport of ILs in a supercooled state is associated with the motion of different types of ions, such as (a) cations: [C₄Him]⁺ and [C₄mim]⁺, (b) anions: [NTf₂]⁻ and [HSO₄]⁻, (c) short or long lived ion-pairs and (d) protons, H⁺ (in case of PILs).
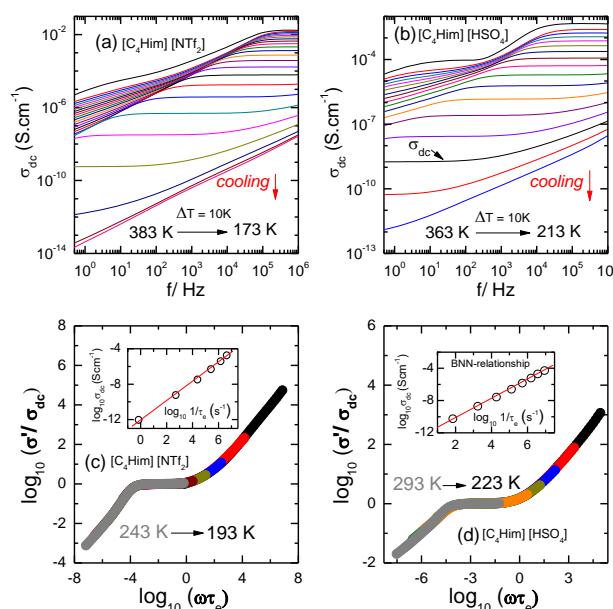

Fig. 3 Frequency dependent conductivity of **(a)** [C₄Him] [NTf₂] and **(b)** [C₄Him] [HSO₄] at several isotherms. Their respective conductivity master curves using Dyre scaling approach are shown in (c) and (d) with BNN relationship for the [C₄Him] [NTf₂] and [C₄Him] [HSO₄], respectively in inset.

In order to examine the charge transport properties, we present the electrical response of ILs in a dynamic window of conductivity formalism. In Figure 3 (a) and (b), the temperature evolution of the real part of conductivity spectra, $\sigma'(f)$ for both protic ionic liquids [C₄Him] [NTf₂] and [C₄Him] [HSO₄] at p = 0.1 MPa have been illustrated. The conductivity data for [C₄mim] [NTf₂] has been reported by us elsewhere.[32] Clearly, $\sigma'(f)$ is characterized by (i) frequency independent conductivity (dc-conductivity, σ_{dc}) seen as a plateau in $\sigma'(f)$ that determines macroscopic long range transport and is proportional to the ion charge, the number of mobile ions and how easily the ion moves through matter,[36] (ii) at higher frequencies, the plateau crosses over to a dispersive regime, where conductivity becomes frequency dependent and obeys power law behaviour i.e., ω^n where n varies from 0.5 to 1.0. Thus, there exists a characteristic frequency that separates the dc-regime with diffusive ionic transport from the dispersive regime described by a sub-diffusive ionic motion. The inverse of the crossover frequency gives a characteristic time (τ_e) of the conductivity process and is proportional to the mobility of charge carriers, (iii) at low frequency and high temperature conditions, a decrease of σ' from σ_{dc} is witnessed. This is due to slowing down of charge carriers at the metal electrodes which is typical for ion conducting materials.[37,38] As a somewhat unintuitive result, the

ARTICLE

intrinsic dc-conductivity of ILs can only be observed at the aforementioned plateau, at frequencies high enough to avoid electrode polarisation effects. We note dc-conductivity (σ_{dc}) and characteristic time (τ_e) as the dynamic observable parameters to describe the charge transport in the examined ILs, thus we proceed to analyse the experimental conductivity data using a theoretical approach developed by Dyre known as random free energy barrier model.[8,20,21,33] In this model, charge carriers hop in a random spatiality with a varying potential energy landscape. The transport is governed by the ability of charge carriers to overcome the randomly distributed energy barriers. The highest barrier that must be overcome to achieve the infinite cluster of hopping sites determines the onset of dc-conductivity with a characteristic time (τ_e) corresponding to the rate to overcome the highest barrier. Within the continuous random walk approximation,[8] the mathematical expression for complex conductivity is given by equation 1:

$$\sigma^*(\upsilon) = \sigma_{dc}\left[\frac{i\omega\tau_e}{\ln(1 + i\omega\tau_e)}\right] \qquad (1)$$

The real part of equation 1 was then used to fit the conductivity data shown in Figures 3(a) and 3(b) for [C$_4$Him] [NTf$_2$] and [C$_4$Him] [HSO$_4$] ILs, respectively, the charge transport mechanism is found to agree with random barrier model. The scaling of the experimental data with respect to estimated quantities at different temperatures yields a single collapsing plot i.e., $\log_{10}$ [$\sigma'(\upsilon)/\sigma_{dc}$] vs. $\log_{10}$ [$\omega\tau_e$], known as the master curve, that is shown in Figures 3(c) and 3(d) for [C$_4$Him] [NTf$_2$] and [C$_4$Him] [HSO$_4$], respectively. It demonstrates that ac and dc charge transport share identical thermal activation, thus a time temperature superposition is obeyed and the Barton-Nakajima-Namikiwa (BNN) relationship is fulfilled (see Figures 3c and 3d inset).[8] The conductivity scaling behaviour of [C$_4$mim] [NTf$_2$] is also satisfied and has been reported by us elsewhere.[32]

To understand the thermal evolution of dc-conductivity, we have plotted the Arrhenius diagram, i.e., $\log_{10}\sigma_{dc}$ as a function of $1000/T$, for all ILs at p = 0.1 MPa in Figure 4(a). It is observed that above T_g, the temperature dependence of conductivity is super-Arrhenius and can be suitably described by Vogel-Fulcher-Tamman (VFT)[39,40,41] equation having the mathematical form:

$$\log_{10}\sigma_{dc} = \log_{10}\sigma_\infty + \frac{DT_0}{T - T_0}\log_{10}\tau_e \qquad (2)$$

where D quantifies the divergence from Arrhenius behaviour, T_0 is the Vogel temperature, and σ_∞ is the dc-conductivity at high temperature. The estimated VFT parameters at 0.1 MPa have been listed in Table 1.
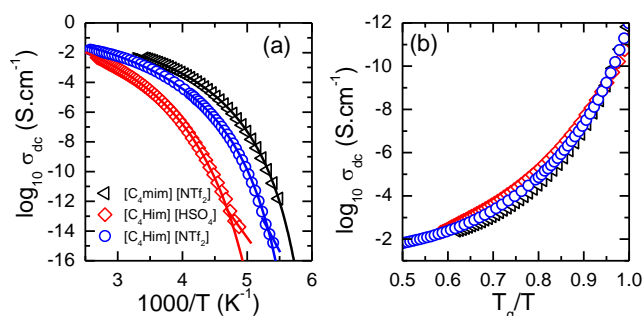

Fig. 4 (a) Thermal evolution of dc-conductivity for all ILs in Arrhenius diagram. The solid lines represent VFT fit to the experimental data. (b) dc-conductivity of ILs as a function of scaled temperature (T_g/T).

The extrapolation to infinite temperature yields a conductivity value close to ~1 S cm^{-1} which has the same order of magnitude as the dc conductivity extrapolated to infinite temperature and resembles those values observed for other fast ionic conductors to saturate at high temperatures.[10] According to convention, the ionic conductivity in a system where ion diffusion is tightly coupled to the structural relaxation is in the order of 10^{-15} S cm^{-1} at T_g.[24] However, in an Arrhenius diagram close to T_g, temperature dependent dc-conductivity reveals a small departure from VFT theoretical locus around ~ 10^{-13} S cm^{-1} for [C$_4$Him] [HSO$_4$] and ~ 10^{-14} S cm^{-1} for [C$_4$Him] [NTf$_2$].[22] These results indicate that the charge transport is slightly decoupled from viscosity in the examined protic ionic liquids. In other words, the mobility of charge carriers is faster than that of the species responsible for structural dynamics. The possible explanation of these observations lies in the fast proton transport through the H-bonded network. Surprisingly, despite slight differences in the value of $\sigma_{dc}(T_g)$ between examined protic ILs we notice that all ILs present similar temperature dependence of dc-conductivity under the super-Arrhenius regime which is reflected through similar divergence values (see Table 1).

Table 1. Temperature dependent VFT fit parameters of dc-conductivity at 0.1 MPa for the [C$_4$Him] [NTf$_2$] and [C$_4$Him] [HSO$_4$] using measured data, as well as for [C$_4$mim] [NTf$_2$] using data from literature.[32]

IL Name	dc-conductivity process			$\left(\dfrac{d\log_{10}\sigma_{dc}}{d\left(\frac{T_g}{T}\right)}\right)_{T=T_g}$	T_g (K)
	$\text{Log}_{10}\sigma_0$ (S cm^{-1})	D	T_0 (K)		
[C$_4$Him] [NTf$_2$]	-0.23 (±0.04)	6.34 (±0.06)	157.21 (±0.40)	72	193
[C$_4$Him] [HSO$_4$]	-0.81 (±0.02)	9.23 (±0.09)	163.87 (±0.39)	63	218
[C$_4$mim] [NTf$_2$]	-0.23 (±0.03)	5.37 (±0.06)	152.86 (±0.21)	78	181.5[35]

	[C4Him] [NTf2]			[C4Him] [HSO4]				[C4mim] [NTf2]		
T (K)	-log σ_0 (S cm^{-1})	$\Delta v^{\#}$ (cm^3 mol^{-1})	T (K)	-log σ_0 (S cm^{-1})	C	p_0 (MPa)	T (K)	-log σ_0 (S cm^{-1})	C	p_0 (MPa)
293	2.87 (±0.01)	23.5 (±0.01)	308	3.75 (±0.01)	27.9 (±3.8)	3951 (±457)	213	5.83 (±0.02)	36.4 (±2.0)	1136 (±46)
313	2.49 (±0.01)	18.7 (±0.06)	314	3.56 (±0.01)	13.6 (±1.6)	2403 (±219)	223	4.96 (±0.02)	31.3 (±1.3)	1302 (±36)
333	2.23 (±0.01)	15.3 (±0.08)	323	3.32 (±0.02)	11.6 (±2.2)	2371 (±343)	233	4.23 (±0.03)	44.8 (±3.5)	2090 (±128)
353	2.05 (±0.01)	12.9 (±0.01)	333	3.06 (±0.01)	51.7 (±29.7)	9913 (±5388)				

Table 2. Pressure dependent Arrhenius and VFT fit parameters of dc-conductivity of selected ILs at given isotherms.

Moreover, we found that all ILs share a common slope magnitude at T_g as shown in Figure 4(b) and reported in Table 1. At this juncture, it is very challenging to distinguish the charge transport properties in the Arrhenius diagram. Thus the key question to be answered is "*how molecular individualities of PILs and AILs reflect and differ through charge transport properties?*". The clue to this problem lies in the elementary aspect of the molecular packing of matter and the ability to form a H-bonded network. Note that pressure as a thermodynamic intensive parameter perturbs molecular packing and intermolecular interaction, thus we expect that isothermal high pressure measurements would resolve the above mentioned problem.

C. Charge transport at elevated pressure

Figures 5(a), 5(b) and 5(c) illustrate the variation of σ_{dc} as a function of pressure (0.1 MPa ≤ p ≤ 600 MPa within a Δp = 50 MPa) at several isotherms for [C4Him] [NTf2], [C4Him] [HSO4] and [C4mim] [NTf2], respectively. It is witnessed that decreasing temperature and increasing pressure both produce a similar effect on the slowing down of the σ_{dc} or mobility of charge carriers.[32,42,43] Interestingly, we distinguish that all three examined ILs reveal a different pressure sensitivity with respect to σ_{dc} which is not resolved in the temperature window, as shown in Figure 4(b). Now we proceed to analyse and describe the pressure activation of σ_{dc} using phenomenological equations.[10] It is observed that in [C4Him] [NTf2], σ_{dc} evolves linearly as a function of pressure for all isotherms and can be suitably described by a simple volume activated law,[9] expressed using equation 3:

$$\log_{10} \sigma_{dc}(p) = \log_{10} \sigma_0 + \frac{p\Delta v^{\#}}{RT} \qquad (3)$$

where $\log_{10}\sigma_0$ is the value of σ_{dc} at $p = 0.1$ MPa, R is the universal gas constant and $\Delta v^{\#}$ is the apparent activation volume. The value of $\Delta v^{\#}$ of [C4Him] [NTf2] for investigated isotherms has been listed in Table 2 and varies from 24 to 13 cm^3 mol^{-1} for all temperatures. It shows that with a rise in temperature, $\Delta v^{\#}$ decreases. This physically implies that local volume expansion required for ionic transport is reduced at high temperatures.

On the contrary, both [C4Him] [HSO4] and [C4mim] [NTf2] show non-linear evolution of σ_{dc} as a function of pressure at all

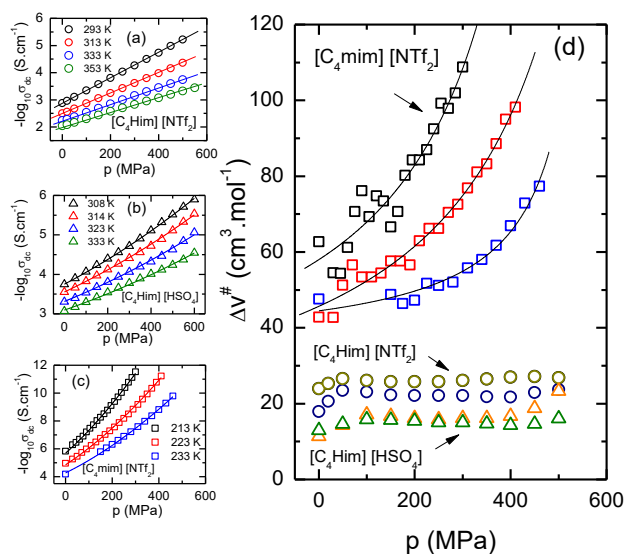Fig. 5 The pressure activation of dc-conductivity for (a) [C4Him] [NTf2], and (b) [C4Him] [HSO4] and (c) [C4mim] [NTf2]. The solid lines represent the fits to eq.3 and eq.4 to the experimental data. (d) The activation volume as a function of pressure for all ILs.

temperatures. Moreover, the pressure sensitivity in the former sample (T = 314 K, $\Delta\sigma_{dc} ≈ 2$ decades) is substantially reduced compared to the latter IL (T = 223 K, $\Delta\sigma_{dc} ≈ 6$ decades). This non-linear increase of σ_{dc} can be described by a pressure counterpart of the VFT equation represented by[9]

$$\log_{10} \sigma_{dc}(p) = \log_{10} \sigma_0 + \frac{Cp}{p_0 - p}\log_{10} e \qquad (4)$$

Analogous to the equation 3, the pressure counterpart of VFT relation comprises three fitting parameters: $\log\sigma_0$, C and p_0. The pre-exponential factor $\log_{10}\sigma_0$, denotes the value of σ_{dc} at ambient pressure, p_0 is the pressure of the ideal glass transition at a constant temperature, C is a dimensionless parameter defined analogously to D reported in the equation 2. The fitted parameters to equation 4 are also listed in Table 2. This nonlinear pressure evolution of σ_{dc} observed in the supercooled liquid state implies that for [C4Him] [HSO4] and [C4mim] [NTf2], $\Delta v^{\#}$ is not constant but it increases with pressure. This is analogous to the activation energy that starts to rise explosively when glass transition is reached by an isobaric cooling approach.[7] The simple relation connecting $\Delta v^{\#}$ and σ_{dc} is given by the equation 5:

ARTICLE

$$\Delta v^{\#} = 2.303RT \left(\frac{d \, \log_{10} \sigma_{dc}}{dp} \right)_T \qquad (5)$$

From equation 5 it is clear that the higher the $\Delta v^{\#}$ value is, the greater is the change in σ_{dc} upon compression. Clearly, the $\Delta v^{\#}$ parameter can be used as a measure of pressure sensitivity of an ionic system. In the present experimental data and as shown in Figure 5d, in the protic IL [C$_4$Him] [HSO$_4$], $\Delta v^{\#}$ varies from 10 to 20 cm^3 mol^{-1} for all isotherms and remains almost constant with increase in pressure. For the aprotic IL [C$_4$mim] [NTf$_2$], $\Delta v^{\#}$ changes non-linearly from 40 cm^3 mol^{-1} to 120 cm^3 mol^{-1} as a function of pressure.

Certainly, $\Delta v^{\#}$ is a very suitable dynamical parameter to understand the relaxation processes in glass-forming liquids.[7] In the framework of the transition state theory, $\Delta v^{\#}$ corresponds to the difference between the volumes occupied by a molecule in transition state and ground states.[7,8,9] Thus, the magnitude of $\Delta v^{\#}$ is expected to reflect the volume required for local molecular motion.[9] Nevertheless, it has been shown that the connection between molecular size and $\Delta v^{\#}$ in ILs is not so straightforward. The relation between $\Delta v^{\#}$ and size of charge carriers thus requires the consideration of many additional factors. These are (i) electrostatic interactions among ion pairs (ii) competition between the van der Waals and electrostatic interactions (iii) ability of ILs to form a H-bonded network and (iv) type of charge carrier. As it has been shown above, the magnitude of $\Delta v^{\#}$ in the examined aprotic IL is sufficiently higher compared to both protic ILs. Thus, the differences between the charge transport properties in PILs and AILs are naturally expected. Specifically, because of the lowest values of $\Delta v^{\#}$, [C$_4$Him] [HSO$_4$] is expected to reveal the most efficient proton transport through the most expanded H-bonded network. To verify these speculations we have employed COSMOthermX calculations.

D. Charge transport in PIL and AIL in the light of theoretical considerations

To investigate the charge transport in the studied ILs at the molecular level we have employed COSMOthermX calculations. As reported in the Table S2 of the ESI, it appears that the COSMO volume of ions increases as follows: [HSO$_4$]$^-$ (87.6 Å^3) < [C$_4$Him]$^+$ (171.5 Å^3) < [C$_4$mim]$^+$ (196.5 Å^3) < [NTf$_2$]$^-$ (196.5 Å^3). This result is fully in agreement with several literature reports.[27,28,29] Furthermore, it is also clear by looking at their sigma profile that the charge on the [HSO$_4$]$^-$ anion is more localized than that on the [NTf$_2$]$^-$ which may induce a greater ability to form ion pairs with selected cations. This has been verified by determining the optimized 3D structure of an ion pair for each selected PIL. From these data, it appears that the [HSO$_4$]$^-$ anion is closer to the [C$_4$Him]$^+$ (minimum distance between the anion-cation = 1.758 Å) reflecting stronger interactions between these ions than those expected between [NTf$_2$]$^-$ and [C$_4$Him]$^+$ (minimum distance between the anion-cation = 1.896 Å). As a consequence the proton hopping between the two protic entities [C$_4$Him]$^+$ and [HSO$_4$]$^-$ is much more efficient than between the same protic cation and the

aprotic [NTf$_2$]$^-$ anion. Such a tendency is also related to the presence of a labile proton on the [HSO$_4$]$^-$ structure enhancing in fact the localisation of the negative charge on the −O-SO$_3^-$ moiety (see Table 2 - ESI) and thus the proton hopping between all ions present in solution. In contrary, in the case of the [C$_4$Him] [NTf$_2$], the proton hopping is solely driven through cation-cation interactions (and distance) which are enhanced in the presence case by its chromonic structure involving pi–pi stacking interactions. Furthermore, the [HSO$_4$]$^-$ anion seems to strongly interact with the acidic hydrogen atom N-H$^+$ of [C$_4$Him]$^+$ in contrary to the [NTf$_2$]$^-$ anion which seems to interact with the [C$_4$Him]$^+$ cation thanks to O-H bonded networks between its oxygen atoms and acid hydrogen atoms N-H$^+$ and the C$_2$ position of [C$_4$Him]$^+$. This tendency is further influenced by looking at the interactions between the [NTf$_2$]$^-$ anion and the [C$_4$mim]$^+$ cation (minimum distance between the anion-cation = 2.179 Å) based on which the [NTf$_2$]$^-$ seems to be highly localized close to the C$_2$ position of [C$_4$mim]$^+$.

Note that generally both protic ILs, [C$_4$Him] [NTf$_2$] and [C$_4$Him] [HSO$_4$], have a higher tendency to form a well-expanded H-bonded network compared to the aprotic [C$_4$mim] [NTf$_2$] material. In a protic IL, the proton is coupled to [C$_4$Him]$^+$ cation.[7,18,19] The proton is the only ion which has no electron shell of its own. Consequently, it strongly interacts with the electron density of its environment. Aside from the above aspect, the examined ILs show a difference in the molecular ion size. Thus, owing to the large volume and asymmetric geometry of the organic cation, charge delocalization (lower degree of charge ordering) takes place, thus reducing the electrostatic interaction due to larger ion-ion distance.[25,26,27,28,29] As a result, local charge ordering extends to several coordination shells in the ionic systems and each ion is surrounded by several counter ions in the first coordination shell forming a "*local ion cage*".[44] The cage structure averaging over all the local cage structures statistically describes the structure and dynamics of an IL in the supercooled state. In particular, a smaller cage volume corresponds to higher density and thus a more stable cage leads to slower dynamics. According to our calculations and these literature reports, the distance between cation and anion changes, thus the columbic interaction roughly follows the increasing trend [C$_4$mim] [NTf$_2$] → [C$_4$Him] [NTf$_2$] → [C$_4$Him] [HSO$_4$] (see Table S2 of ESI). Note that in the [C$_4$Him] [NTf$_2$] protic ILs, the proton is attached to the cation and at elevated pressures the proton H$^+$ strongly interacts with its environment due to cluster formation (more packed H-bonded networks) and moves through H-bonded network. Similar tendency could be patented in the case of the [C$_4$Him] [HSO$_4$] while greater H-bonded networks are expected due to the protic nature of both the anion and cation, which is not the case, of course, of the [C$_4$mim] [NTf$_2$] aprotic IL. Thus, it is translated as an increase in dc-conductivity of the system and significant drop in $\Delta v^{\#}$ takes place in protic (by respecting also the ions structure leading to a lower value of $\Delta v^{\#}$ for protic-protic, *e.g.* [C$_4$Him] [HSO$_4$] than for protic-aprotic, *e.g.* [C$_4$Him] [NTf$_2$] ionic liquids) *vs.* aprotic ILs (*e.g.* [C$_4$mim] [NTf$_2$]). Congruently, high pressure investigations on protic ILs establish that when the ionic conduction process is

dominated by the smallest charge carriers (such as protons), the value of $\Delta v^{\#}$ significantly decreases.[23] For instance, in carvedilol salts $\Delta v^{\#}$ becomes two times lower when the anion is changed from hydrochloride (131 cm^3 mol^{-1}) to phosphate (62 cm^3 mol^{-1}) due to the Grotthuss mechanism. As a result, $\Delta v^{\#}$ of protic ILs are significantly lower than those of AILs. Thus, we note that the strength of the hydrogen bond network, proton transfer and conduction mechanism amply and influence the magnitude of $\Delta v^{\#}$. At this juncture, we establish that $\Delta v^{\#}$ is a method to resolve and separate the charge transport properties of PILs from AILs using high pressure, a technique which is not possible using a temperature window.

Conclusions

Using broadband dielectric spectroscopy, we have measured the dc-conductivity of the [C$_4$Him] [NTf$_2$], [C$_4$Him] [HSO$_4$] and [C$_4$mim] [NTf$_2$] ILs over a broad range of temperatures and pressures. The frequency dependent conductivity data were analysed using the free energy random barrier model and established a time-temperature superposition. It also demonstrates that ac and dc charge transport have identical thermal activation barriers. All examined ILs reveal a similar temperature dependence on dc-conductivity behaviour close to glass transition. The role of molecular conformation on transport properties has been discussed. Intriguingly, high pressure studies show a different pressure sensitivity on dc-conductivity which is not resolved in a temperature window. We establish that the activation volume can be used as a measure of pressure sensitivity of an ionic system and its ability to from a H-bonded network, which may be associated with results obtained from the COSMOthermX software such as sigma profile and free volume of each species. In conclusion, a connection between activation volume and proton transfer has been established. Finally, we note that pressure can be used as a suitable parameter to distinguish the charge transport mechanism of ionic liquids according to the structure of their ions in solutions from PILs (based on a protic cation and a protic or an aprotic anion) to AILs.

AUTHOR INFORMATION

The authors declare no competing financial interest.

ACKNOWLEDGEMENT

References

1 C. A. Angell, Y. Ansari and Z. Zhao, *Faraday Discuss.*, 2012, **154** (1), 9–27.
2 A. Kumar Gupta, R. Kumar Singh, S. Chandra *Ionics*, 2014, **20**, 507–516.
3 D. R. MacFarlane, N. Tachikawa, M. Forsyth, J. M. Pringle, P.C. Howlett, G.D. Elliott, J. H. Davis, M. Watanabe, B. Simon and C. A. Angell, *Energy Environ. Sci.*, 2014, **7** (1), 232–250.
4 K. L. Ngai, *J. Phys. Condens. Matter*, 2003, **15** (11), S1107–S1125.
5 H. K. Kashyap, H. V. R. Annapureddy, F. O. Raineri and C. J. Margulis, *J. Phys. Chem. B*, 2011, **115** (45), 13212–13221.
6 W. Xu, E. I. Cooper and C. A. Angell, *J. Phys. Chem. B*, 2003, **107** (25), 6170–6178.
7 M. Paluch, *Dielectric Properties of Ionic Liquids*; M. Paluch, Ed.; Advances in Dielectrics; Springer International Publishing: Cham, 2016.
8 F. Kremer and A. Schönhals, *Broadband Dielectric Spectroscopy*; F. Kremer and A. Schönhals, Eds.; Springer Berlin Heidelberg: Berlin, Heidelberg, 2003.
9 G. Floudas, M. Paluch, A. Grzybowski and K. L. Ngai, *Molecular Dynamics of Glass-Forming Systems*; Advances in Dielectrics; Springer Berlin Heidelberg: Berlin, Heidelberg, 2011.
10 K. L. Ngai, *Igarss 2014* 2011, No. **1**, 1–5.
11 B. Kirchner, *Ionic Liquids*; B. Kirchner, Ed.; Springer Berlin Heidelberg: Berlin, Heidelberg, 2010.
12 H. Weingärtner, *Angew. Chem. Int. Ed.*, 2008, **47**, 654–670.
13 H. Ohno, *Electrochemical Aspects of Ionic Liquids*; H. Ohno, Ed.; John Wiley & Sons, Inc.: Hoboken, NJ, USA, 2005.
14 P. Simon and Y. Gogotsi, *Nature Mater.*, 2008, **7**, 845-854.
15 Michel Armand, Frank Endres, D. R. MacFarlane, H. Ohno and B. Scrosati, *Nature Materials*, 2009, **8**, 621 – 629.
16 A. S. Amarasekara, *Chem. Rev.*, 2016, **116** (10), 6133–6183.
17 A. Mirjafari, L. N. Pham, J. R. McCabe, N. Mobarrez, E. A. Salter, A. Wierzbicki, K. N. West, R. E. Sykora and J. H. Davis, *RSC Adv.*, 2013, 3 (2), 337–340.
18 Z. Wojnarowska and M. Paluch, *J. Phys. Condens. Matter*, 2015, **27** (7), 073202.
19 T. L. Greaves and C. J. Drummond, *Chem. Rev.* 2015, **115** (20), 11379–11448.
20 T. Cosby, A. Holt, P. J. Griffin, Y. Wang and J. Sangoro, *J. Phys. Chem. Lett.* 2015, **6** (19), 3961–3965.
21 J. R. Sangoro, C. Iacob, A. Serghei, C. Friedrich and F. Kremer, *Phys. Chem. Chem. Phys.* 2009, **11** (6), 913–916.
22 P. Griffin, A. L. Agapov, A. Kisliuk, X.-G. Sun, S. Dai, V. N. Novikov and A. P. Sokolov, *J. Chem. Phys.* 2011, **135** (11), 114509.
23 Z. Wojnarowska, Y. Wang, J. Pionteck, K. Grzybowska, A. P. Sokolov and M. Paluch, *Phys. Rev. Lett.* 2013, **111** (22), 225703.
24 Z. Wojnarowska, J. Knapik, M. Díaz, A. Ortiz, I. Ortiz, and M. Paluch, *Macromolecules* 2014, **47** (12), 4056–4065.
25 S. Tsuzuki, H. Tokuda, K. Hayamizu, and M. Watanabe, *J. Phys. Chem. B* 2005, **109** (34), 16474–16481.
26 H. V. Spohr and G. N. Patey, *J. Chem. Phys.* 2010, **132** (23), 234510.
27 K. R. Ramya, P. Kumar and A. Venkatnathan, *J. Phys. Chem. B* 2015, **119** (46), 14800–14806.
28 S. Zhang, N. Sun, X. He, X. Lu and X. Zhang, *J. Phys. Chem. Ref. Data* 2006, **35** (4), 1475.
29 M. G. Montalbán, C. L. Bolívar, F. G. Díaz Baños and G. Víllora, *J. Chem. Eng. Data* 2015, **60** (7), 1986–1996.
30 J. Habasaki and K. L. Ngai, *J. Chem. Phys.* 2008, **129** (19), 194501.
31 A. Rivera and E. A. Rössler, *Phys. Rev. B* 2006, **73** (21), 212201.
32 Z. Wojnarowska, G. Jarosz, A. Grzybowski, J. Pionteck, J. Jacquemin and M. Paluch, *Phys. Chem. Chem. Phys.* 2014, **16** (38), 20444–20450.
33 J. C. Dyre, *J. Appl. Phys.* 1988, **64** (5), 2456–2468.
34 A. R. Neale, P. Li, J. Jacquemin, P. Goodrich, S. Ball, R. G. Compton and C. Hardacre, *Phys. Chem. Chem. Phys.* 2016, **18** (16), 11251–11262.

35 A. V. Blokhin, Y. U. Paulechka, A. A. Strechan and G. J. Kabo, *J. Phys. Chem. B* 2008, **112** (14), 4357–4364.

36 J. C. Dyre, P. Maass, B. Roling and D. L. Sidebottom, *Reports Prog. Phys.* 2009, **72** (4), 046501.

37 A. Serghei, M. Tress, J. R. Sangoro and F. Kremer, *Phys. Rev. B* 2009, **80** (18), 184301.

38 S. N. Tripathy, Z. Wojnarowska, J. Knapik, H. Shirota, R. Biswas and M. Paluch, *J. Chem. Phys.* 2015, **142** (18), 184504.

39 H. Vogel, *Phys. Z.* 1921, **222**, 645.

40 G. S. Fulcher, *J. Am. Ceram. Soc* 1925, **8** (6), 789–794.

41 G. Tammann and W. Hesse, *Zeitschrift für Anorg. und Allg. Chemie* 1926, **156** (1), 245–257.

42 G. Jarosz, M. Mierzwa, J. Ziozo, M. Paluch, H. Shirota and K. L. Ngai, *J. Phys. Chem. B* 2011, **115**, 12709–12716.

43 M. Paluch, Z. Wojnarowska, P. Goodrich, J. Jacquemin, J. Pionteck and S. Hensel-Bielowka, *Soft Matter* 2015, **11** (32), 6520–6526.

44 R. Shi and Y. Wang, *Sci. Rep.* 2016, **6**, 19644.